crystals

MDPI

Article

Study on the Growth and Regulation of Large-Particle $Sr(OH)_2·8H_2O$ Crystals with Process Analytical Technology

Binbin Shi [1,2,3], Yongjuan Zhang [2], Shudong Liang [2], Yanan Wang [1,2], Yan Jing [1,2], Xingwu Zou [1,2,*] and Xuezhong Wang [4,*]

[1] Key Laboratory of Comprehensive and Highly Efficient Utilization of Salt Lake Resources, Qinghai Institute of Salt Lakes, Chinese Academy of Sciences, Xining 810008, China; shibinbin22@mails.ucas.ac.cn (B.S.); wyn_0607@163.com (Y.W.); jingyan@isl.ac.cn (Y.J.)
[2] Qinghai Engineering and Technology Research Center of Comprehensive Utilization of Salt Lake Resources, Xining 810008, China; zhangyongjuan1212@163.com (Y.Z.); 18797364518@163.com (S.L.)
[3] University of Chinese Academy of Sciences, Beijing 100049, China
[4] School of Chemical and Process Engineering, University of Leeds, Leeds LS2 9JT, UK
* Correspondence: zouxingwu@isl.ac.cn (X.Z.); X.Z.Wang@Leeds.ac.uk (X.W.)

Abstract: $Sr(OH)_2$ is an indispensable strontium compound extensively harnessed in sugar refining, strontium lubricating wax formulation, and polymer plastic stabilization. $Sr(OH)_2·8H_2O$ is the prevalent hydrate form of $Sr(OH)_2$. Deprived of moisture via vacuum drying, $Sr(OH)_2$ can be procured from $Sr(OH)_2·8H_2O$. $Sr(OH)_2·8H_2O$ particles with larger sizes exhibit impressive attributes such as facile solid–liquid divergence, elevated product purity, expedient drying, and resilience to agglomeration, which have garnered significant interest. Given the superior quality of the product and the dependability of the process, process analytical technology (PAT) has been extensively employed in the pharmaceutical sector, rendering it feasible to employ PAT to fabricate large-particle $Sr(OH)_2·8H_2O$ crystals. This study utilizes industrial $SrCO_3$ to prepare high-purity $Sr(OH)_2·8H_2O$ with a purity of over 99.5%. The growth process of single crystals was observed using a hot-stage microscope, and the growth process of large-particle $Sr(OH)_2·8H_2O$ was optimized and regulated online using PAT. The optimal process conditions were optimized, and large-particle $Sr(OH)_2·8H_2O$ crystals were obtained by adding crystal seeds. On this basis, we proposed a seed control mechanism for $Sr(OH)_2·8H_2O$.

Keywords: $Sr(OH)_2·8H_2O$; process analytical technology; crystal growth; seed control

check for updates

Citation: Shi, B.; Zhang, Y.; Liang, S.; Wang, Y.; Jing, Y.; Zou, X.; Wang, X. Study on the Growth and Regulation of Large-Particle $Sr(OH)_2·8H_2O$ Crystals with Process Analytical Technology. *Crystals* **2024**, *14*, 4. https://doi.org/10.3390/cryst14010004

Academic Editor: Andrey Prokofiev

Received: 26 November 2023
Revised: 13 December 2023
Accepted: 18 December 2023
Published: 20 December 2023

Copyright: © 2023 by the authors. Licensee MDPI, Basel, Switzerland. This article is an open access article distributed under the terms and conditions of the Creative Commons Attribution (CC BY) license (https://creativecommons.org/licenses/by/4.0/).

1. Introduction

Crystallization is one of the most traditional operations in separation and purification [1]. Owing to its superior efficiency, reduced energy consumption, and minimal environmental impact, it is used in the production of most chemical solid materials in industry [2]. In food, pharmaceuticals, and fine chemicals, the production and recovery processes of various initial products, by-products, intermediates, and products cannot be separated from crystallization processes [3–9]. The crystallization process determines various characteristics of solid products, including morphology, size, crystal form, and purity, which have a significant impact on their physical and chemical properties [10]. Therefore, the current research focus is primarily on obtaining high-value, high-quality, and highly bioavailable crystals through crystal regulation to satisfy the requirements of industrial production [11]. Despite limited technological advancements and low popularity in the industrial field, the crystallization process still needs to be better understood as a unit procedure due to the complicated mechanisms of nucleation and growth involved. Process analytical technology (PAT) ensures the quality of the final product and the reliability of the investigation process through operational monitoring, analysis, and regulating experimental parameters [12,13]. By using PAT for online monitoring of the crystallization

process, it is feasible to better comprehend the impact of the crystallization process on vital characteristics of crystal products, such as purity, particle size, shape, crystal form, etc., and to comprehend better the thermodynamic boundaries and nucleation growth kinetics of the crystallization process to explore the crystal growth mechanism [14–16].

$Sr(OH)_2$ represents a key strontium compound extensively harnessed in sugar refining, strontium lubricating wax synthesis, and polymer plastic stabilization [17–19]. Moreover, $Sr(OH)_2$ is available to remove deep metal impurities under alkaline conditions and is frequently used to prepare downstream high-purity strontium salt products. It has even initiated a vital platform product for the entire strontium industry chain, supplanting primary strontium salt products such as $SrCl_2$ and $SrCO_3$. $Sr(OH)_2{\cdot}8H_2O$ is the prevalent hydrate form of $Sr(OH)_2$. Deprived of moisture via vacuum drying, $Sr(OH)_2$ can be procured from $Sr(OH)_2{\cdot}8H_2O$. Particles with larger sizes have excellent characteristics such as convenient solid–liquid separation, high product purity, convenient drying, and resistance to clumping, which have attracted much attention. Despite this, the current research on the crystal size regulation of $Sr(OH)_2{\cdot}8H_2O$ is not comprehensive enough, and the quality of $Sr(OH)_2{\cdot}8H_2O$ products available on the market is not high, which is primarily manifested as irregular particle shape, delicate crystal particles, and high impurity content. As the strontium salt industry evolves, the production of $Sr(OH)_2{\cdot}8H_2O$ is progressively enhancing in both quality and quantity, and the demand for large-particle $Sr(OH)_2{\cdot}8H_2O$ products is escalating [20]. The superior quality and dependability of products prepared based on PAT have resulted in them being extensively employed in the pharmaceutical field, making it feasible to manufacture large-particle $Sr(OH)_2{\cdot}8H_2O$ crystals employing PAT.

In this work, we prepared high-purity $Sr(OH)_2{\cdot}8H_2O$ with a purity of over 99.5% using industrial $SrCO_3$ as raw material. Subsequently, the growth process of the single crystal was observed utilizing a hot-stage microscope, and multiple PATs were integrated to in situ measure and regulate the growth process of large-particle $Sr(OH)_2{\cdot}8H_2O$. Ultimately, the large-particle $Sr(OH)_2{\cdot}8H_2O$ crystal was prepared by adding seeds; based on this, the seed regulation mechanism of $Sr(OH)_2{\cdot}8H_2O$ was explored.

2. Materials and Methods

2.1. Materials

The $Sr(OH)_2{\cdot}8H_2O$ used in this research was prepared industrially through calcination, water immersion, and recrystallization. Industrial $SrCO_3$ was calcined at 1250 °C to achieve a weight loss rate of over 99% and then reacted with ultrapure water to obtain a $Sr(OH)_2$ slurry (with a mass ratio of SrO to the water of 1:8). After boiling and filtering, a hot $Sr(OH)_2$ solution was obtained. Subsequently, it was cooled and crystallized, and solid–liquid separation was carried out to obtain the crude $Sr(OH)_2{\cdot}8H_2O$ initial product. The mass ratio of $Sr(OH)_2$ to deionized water was 1:5, and refined $Sr(OH)_2{\cdot}8H_2O$ was obtained through two recrystallizations, which were then vacuum dried at 60 °C. The solvent used for preparing the solution was ultrapure water, obtained via the Beijing Youpu Pure Water Mechanism. Subsequently, after grinding, particle size classification was achieved via sieving of crystal seeds utilizing 80 mesh (180 μm), 120 mesh (125 μm), 160 mesh (96 μm), and 200 mesh (75 μm) screens.

2.2. $Sr(OH)_2{\cdot}8H_2O$ Hot-Stage Growth Process

A polarizing microscope (Olympus BX53, Olympus, Tokyo, Japan) was employed to scrutinize the growth progression of $Sr(OH)_2{\cdot}8H_2O$ crystals, concurrently ensuring meticulous control of the temperature of crystal development via a hot-stage apparatus (LNP95, Beijing AidiJiaye Development Co., Ltd., Beijing, China). First, a saturated $Sr(OH)_2$ solution was prepared at 25 °C and placed in the hot-stage reactor. From the solubility curve of the $Sr(OH)_2{\cdot}8H_2O$-H_2O system in Figure 1, it can be seen that the solubility of $Sr(OH)_2{\cdot}8H_2O$

at 20 °C is 1.77 g/100g H_2O [21]. Based on the above conditions, $Sr(OH)_2{\cdot}8H_2O$ solutions with different relative supersaturations were prepared according to the following equation:

$$\sigma = (C - C^*)/C^*$$

where σ denotes the solution's relative supersaturation, C denotes the solution's actual concentration, and C^* denotes the equilibrium saturation concentration at that temperature. Subsequently, a self-made $Sr(OH)_2{\cdot}8H_2O$ crystal was selected and added to a saturated solution. It was covered with a circular cover glass and the temperature was adjusted to 20 °C. Once operational, the polarizing microscope captured snapshots every 10 s.

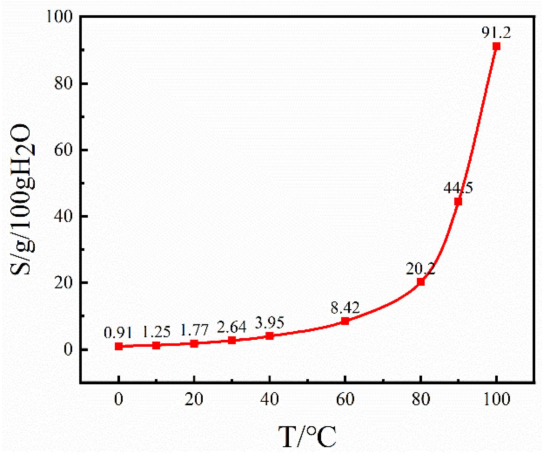


Figure 1. $Sr(OH)_2{\cdot}8H_2O$ solubility curve in $Sr(OH)_2{\cdot}8H_2O$-H_2O system.

2.3. Online Analysis of the Crystallization Process of $Sr(OH)_2{\cdot}8H_2O$

In this work, we synthesized large-particle $Sr(OH)_2{\cdot}8H_2O$ crystals primarily through the cooling crystallization process in a 2 L jacket reactor. Initially, 1.5 L of $Sr(OH)_2{\cdot}8H_2O$ supersaturated solutions were prepared with varied initial supersaturations based on the 20 °C saturation concentration. Subsequently, at divergent stirring rates, the $Sr(OH)_2{\cdot}8H_2O$ crystal slurry was gradually cooled to 20 °C at diverse cooling rates and incubated at this temperature for a period of time. Following crystallization, the $Sr(OH)_2{\cdot}8H_2O$ crystal slurry was solid–liquid fractionated. Post-vacuum drying, the final $Sr(OH)_2{\cdot}8H_2O$ product was acquired. The complexity of this process is primarily due to the need to coordinate and optimize multiple parameters: initial supersaturation, cooling rate, stirring rate, and crystal growing time. Furthermore, crystal seeds are added during the cooling crystallization process to suppress secondary nucleation and eliminate induced nucleation. Crystal seeds regulate the particle size of $Sr(OH)_2{\cdot}8H_2O$.

The 2 L reaction device configured for the refrigeration crystallization procedure is illustrated in Figure 2. A constant-temperature water bath (Julabo CF41, Julabo, Seelbach (Black Forest), Germany) precisely managed the crystallization temperature, complemented by an overhead agitator (ChemTron OHS.1D, Julabo, Seelbach (Black Forest), Germany) for consistent mixing. We employed a four-blade tilting stirrer with a 3 cm radius as the stirring paddle. A platinum resistance thermometer (PT100) served as our primary temperature gauge. A turbidity detector (TP-17V1-001, Qingdao Lattice Intelligent Technology Co., Ltd., Qingdao, China) was employed to track variations in solution turbidity. Observations on the crystallization progression were facilitated with a 2D imaging microscopy probe (2DVP-17V16, Qingdao Lattice Intelligent Technology Co., Ltd., Qingdao, China). The probe is intruded into the solution; the probe is equipped with a built-in microscope camera, which can easily take real-time photos and connect to dedicated software called Stereo Vision to record crystal morphology images [22–24]. Lastly, the ultrasonic particle size measurement probe (NS-S 17S-001, Qingdao Lattice Intelligent Technology Co., Ltd., Qingdao, China) is deployed to assess the particle dimension of crystals in solution. Upon employing this

ultrasonic particle sizer, the particle size and dispersion within solutions are influenced by sound wave transmission. The ultrasonic attenuation of test specimens is harnessed for immediate particle sizing data [25]. A cooling crystallization process for $Sr(OH)_2 \cdot 8H_2O$ was conducted in a 2 L jacket reactor, with an initial volume of 1.5 L of $Sr(OH)_2 \cdot 8H_2O$ solution prepared for the experiment.

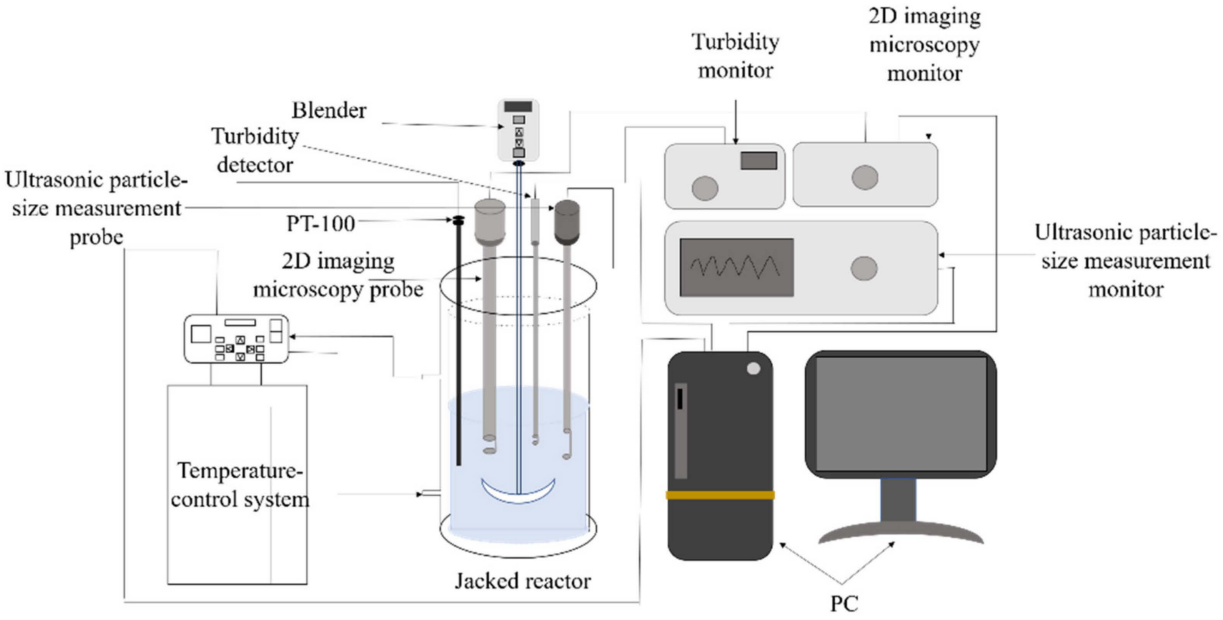


Figure 2. Online analytical apparatus for the $Sr(OH)_2 \cdot 8H_2O$ crystallization procedure.

2.4. Characterization

We employed an X-ray diffractometer (D8 Discover, Bruker, Karlsruhe, Germany) to ascertain the structure of the fabricated $Sr(OH)_2 \cdot 8H_2O$ crystal. A thermogravimetric analyzer (Thermal Analyzer, Themys, Roquevaire, France) was utilized to determine the quantity of crystalline water present in the sample.

3. Results and Discussion

3.1. Phase Identification

The solubility of $Sr(OH)_2$ in pure water varies with the content of H_2O in the crystal structure. Therefore, it is necessary to ensure the crystal structure and the amount of crystal water it contains. The crystal structure of the prepared product was analyzed via XRD. As shown in Figure 3a, it was found that the diffraction peak of the crystal sample is consistent with $Sr(OH)_2 \cdot 8H_2O$ (JCPDS no. 75-0202), indicating that there were no additional components in the $Sr(OH)_2 \cdot 8H_2O$ crystal prepared during the dissolution crystallization process. It can be seen from Figure 3b that the first plateau zone appeared at 128.1 °C with a weight loss of 54.83%. When the temperature continued to rise to 518.2 °C, a second plateau zone can be observed with a weight loss of 5.42% again. After analysis, it can be concluded that the first platform is the process of losing all crystalline water, and the second platform is the process of decomposing strontium hydroxide into strontium oxide. The calculated crystal water in the product is 8.1, which is fairly close to the amount of crystal water in $Sr(OH)_2 \cdot 8H_2O$. It can be considered that the product obtained after the experiment is $Sr(OH)_2 \cdot 8H_2O$.

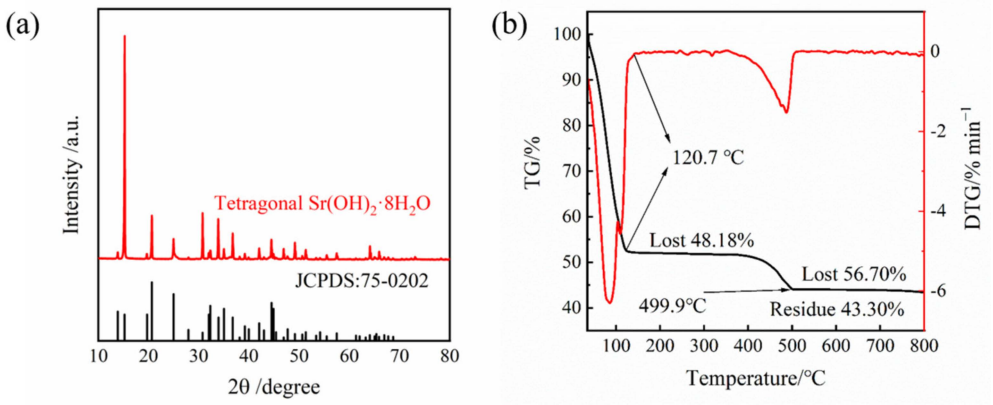


Figure 3. (**a**) XRD pattern of as-prepared $Sr(OH)_2 \cdot 8H_2O$ via recrystallization. (**b**) Mass change curve of the material under progressive temperature rise.

3.2. Single Crystal Hot-Stage Growth

The imaged morphological features of $Sr(OH)_2 \cdot 8H_2O$ during the crystal growth process are illustrated in Figure 4. The entire growth process lasted for 28 min, and the morphological features were collected every 4 min. From Figure 4a–h, it can be observed that with the gradual increase in time, the $Sr(OH)_2$ seed added into the system gradually grew into relatively intact flake crystals. The average growth rate of one seed is 3.25 μm·min^{-1}, which is a considerable growth rate. The reason for this is that in the entire system, only a single $Sr(OH)_2$ crystal exists, and all supersaturations in the saturated solution are used for the growth of this crystal. The crystal growth process observed through a hot-stage microscope provides a method reference for the online growth process of $Sr(OH)_2 \cdot 8H_2O$.

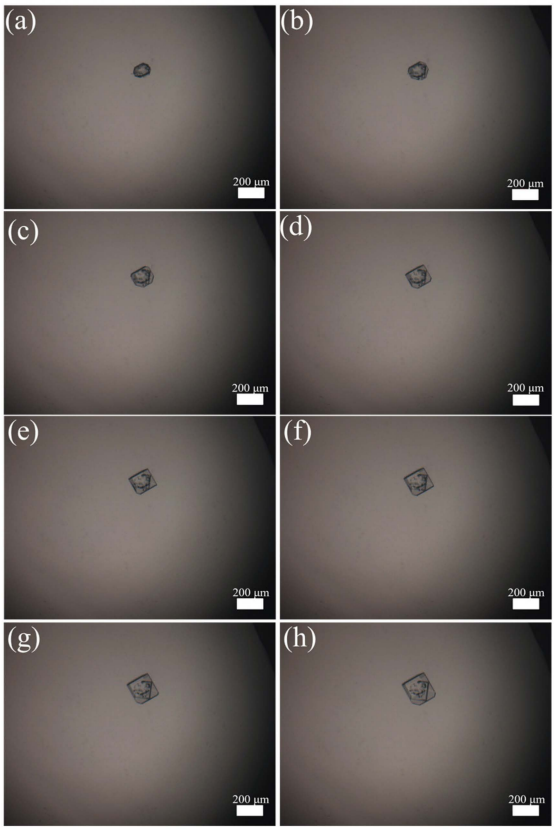


Figure 4. Crystal growth in hot stage: (**a**) 0 min, (**b**) 4 min, (**c**) 8 min, (**d**) 12 min, (**e**) 16 min, (**f**) 20 min, (**g**) 24 min, (**h**) 28 min.

3.3. The Optimal Process without Adding Crystal Seeds

Crystal nucleation and growth are intimately associated with operational parameters such as supersaturation, stirring rate, cooling rate, and crystal growth time. Within this study, the chilling crystallization procedure of $Sr(OH)_2 \cdot 8H_2O$ was manipulated in a jacketed reactor. Hence, this operation is not merely a single crystal nucleation and growth process, but more appropriately described as a process of crystal cluster growth.

From Figure 5a, it can be observed that as the initial relative supersaturation escalates, the D_{50} (median diameter) of $Sr(OH)_2 \cdot 8H_2O$ crystals initially increases and subsequently diminishes, emanating the highest D_{50} at a supersaturation of 3. At lower initial supersaturation levels, the crystal nucleation and growth process is relatively sluggish, leading to a poor crystal production rate. Moreover, when the initial relative supersaturation of the solution is elevated, both crystal nucleation and crystal growth accelerate, leading to a heightened probability of system explosion nucleation and an augmentation in the number of crystals. Due to the competition amongst numerous crystal nuclei, the crystal particle size is smaller [26–29]. Therefore, a suitable initial relative supersaturation is beneficial for the growth of $Sr(OH)_2 \cdot 8H_2O$ crystals.

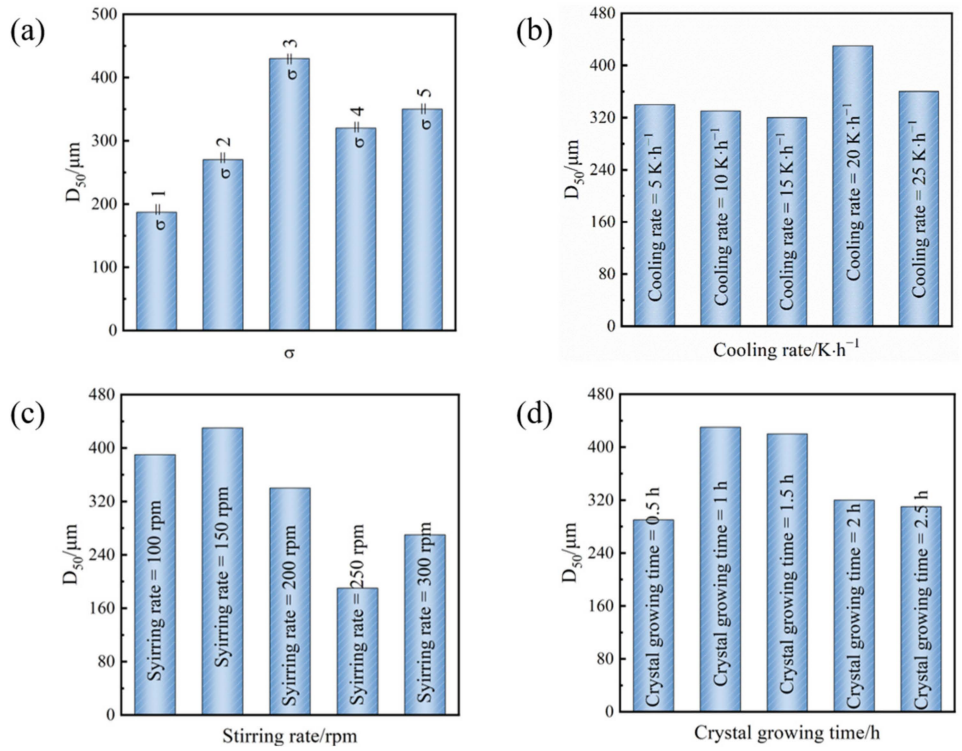


Figure 5. (**a**) At a cooling rate of 20 °C·h^{-1} and a stirring rate of 150 r·min^{-1}, D_{50} of $Sr(OH)_2 \cdot 8H_2O$ crystals at different supersaturations. (**b**) At the initial relative supersaturation of the solution σ = 3 and a stirring rate of 150 r·min^{-1}, D_{50} of $Sr(OH)_2 \cdot 8H_2O$ crystals at different cooling rates. (**c**) At the initial relative supersaturation of the solution σ = 3 and a cooling rate of 20 °C·h^{-1}, D_{50} of $Sr(OH)_2 \cdot 8H_2O$ crystals at different stirring rates. (**d**) At the initial relative supersaturation of the solution σ = 3, a cooling rate of 20 °C·h^{-1}, and a stirring rate of 150 r·min^{-1}, D_{50} of $Sr(OH)_2 \cdot 8H_2O$ crystals at different crystallization times.

As shown in Figure 5b, as the cooling rate increases, the D_{50} of the $Sr(OH)_2 \cdot 8H_2O$ crystal exhibits an initial increase followed by a subsequent decrease, corroborating the result in Figure 5a. This system attains its maximum D_{50} at a cooling rate of 20 °C·h^{-1}. During the cooling crystallization process, the cooling rate is directly proportional to the supersaturation of the solution. If the cooling rate is excessively slow, the period it requires for the solution to generate supersaturation is longer, and crystal growth predominates. Meanwhile, due to the inadequate driving force for crystal growth, productivity is reduced.

If the cooling rate is excessively rapid, the supersaturation of the solution escalates. However, crystal growth is not sufficient to consume the accumulation of supersaturation, which can lead to secondary nucleation. Crystals that undergo secondary nucleation compete with existing crystals for supersaturation for their growth, and having multiple nuclei can also induce secondary processes such as crystal collision and fragmentation, ultimately leading to a decrease in crystal size. Notably, at a cooling rate range of 5–15 °C·h^{-1}, the variation in crystal particle size is insignificant. The potential rationale for this phenomenon is that while the cooling elevates the supersaturation of the solution, the magnitude of crystal nucleation and growth within the entire system is equivalent. That is, growth and nucleation tend to balance; hence, the particle size alteration is insignificant. When the cooling rate reaches 20 °C·h^{-1}, crystal growth prevails, and the crystal particle size tends to augment. As the cooling rate amplifies, crystal nucleation starts to dominate again, and the crystal particle size diminishes.

The stirring rate is a crucial operating parameter in the crystallization process, and stirring affects the crystal growth process from two aspects. On the one hand, stirring can enhance the mass transfer process of the system, making the supersaturation distribution of the system uniform. On the other hand, stirring produces a shear-crushing effect [30–32]. When the stirring rate is high, it causes turbulence and increases the shear force, breaking the crystals and obtaining crystals with a broad particle size distribution. Thus, the agitating rate merely necessitates ensuring that the system is thoroughly mixed. Figure 5c illustrates that the ideal pace is 150 rpm.

The objective of crystal cultivation is to isolate minute crystals and continually grow substantial crystal particulates. In an equilibrium system, the solute will eventually grow on the large crystal, resulting in an increase in crystal size [33]. Consequently, an optimal crystal growth span can escalate the crystal dimension and enhance uniformity. Figure 5d displays the morphology and size of $Sr(OH)_2{\cdot}8H_2O$ crystals under diverse crystal growth times. As the crystal growth time increases, the particle size of $Sr(OH)_2{\cdot}8H_2O$ crystals first increases and then decreases. Under one hour of crystal growing time, we achieved the maximum D_{50}. Within a briefer crystal growth time, the alteration in crystal particle dimension attained was insignificant. Considering the fact that the entire process is a stirring operation, if the crystallization time is excessive, the stirring effect can induce crystal disruption.

3.4. PAT under Optimal Process Conditions

Based on the optimal process conditions mentioned above (initial relative supersaturation of solution $\sigma = 3$, the cooling rate is 20.0 °C·h^{-1}, the stirring rate is 150 r·min^{-1}, and the crystal cultivation time is one hour), we conducted an online analysis of the $Sr(OH)_2{\cdot}8H_2O$ growth process. The initial temperature was 55 °C, and the image observed via PAT imaging equipment is shown in Figure 5a. As illustrated in Figure 6b,c and Figure 7, upon the system being subjected to moderate cooling for approximately 20 min, the solution initiated crystallization, culminating in a $Sr(OH)_2{\cdot}8H_2O$ D_{50} of 39.6 μm; the D_{50} at 40 min was 56.4 μm. The above phenomenon is mainly attributed to the high initial supersaturation of the system in the early stage of crystallization, which is mainly nucleation and supplemented by growth, resulting in a smaller crystal size. As the cooling process proceeds, the supersaturation of the system continues to amass, and the supersaturation is consumed with the nucleation and growth of the crystal, hence the crystal progressively grows at this juncture. Over time, the system enters a relatively stable nucleation and crystal growth stage, thereby achieving a final product particle size of 455.6 μm. The growth trend of $Sr(OH)_2{\cdot}8H_2O$ crystals can be seen from the 2D images taken at various time points in Figure 6.

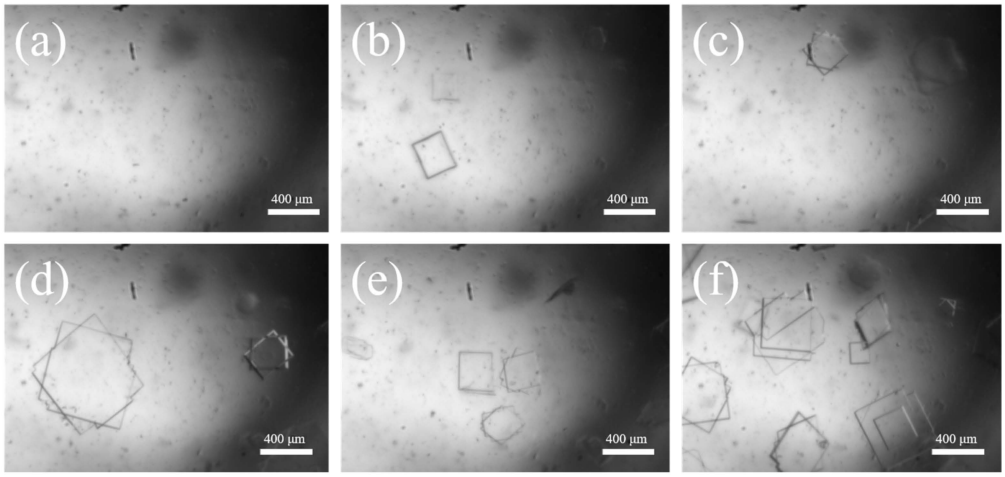


Figure 6. Two-dimensional images of $Sr(OH)_2 \cdot 8H_2O$ under optimal processing conditions and diverse crystallization periods; (**a**) 0 min, (**b**) 20 min, (**c**) 40 min, (**d**) 60 min, (**e**) 80 min, (**f**) 100 min.

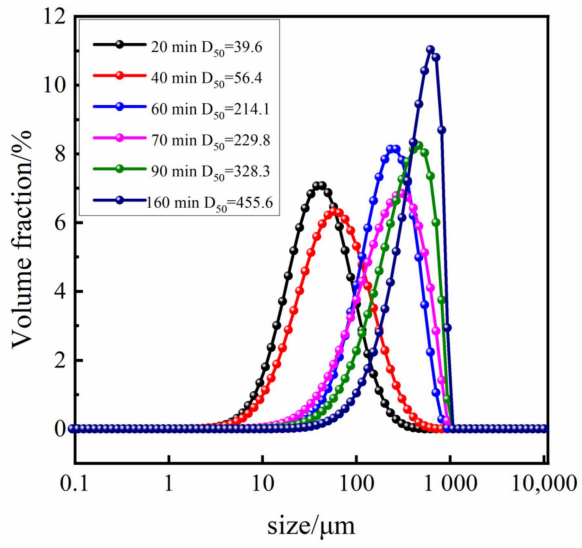


Figure 7. Particle size distribution of $Sr(OH)_2 \cdot 8H_2O$ under optimal process conditions and various crystallization periods.

3.5. The Impact of Crystal Seeds on the Particle Size of $Sr(OH)_2 \cdot 8H_2O$

The incorporation of seed crystals during the crystallization process is recognized as the most desirable method to control the sample size, particularly as a potent strategy to procure crystals with substantial particle dimensions. The seed crystals adsorb nucleation components for their growth; thus, the addition of seed crystals can augment the product particle size [34,35]. On the basis of optimal process conditions, we investigated the influence of crystal seeds on particle size. From Figure 8a, it is evident that as the quantity of seeds introduced escalates, the crystal size of $Sr(OH)_2 \cdot 8H_2O$ initially rises and subsequently diminishes, yet the overall particle size is more considerable than that achieved via the non-seed process. When the number of crystal seeds added is 3 wt%, the maximum particle size of the product is 945 μm. Inclusion of a lesser quantity of seeds will spur the spontaneous nucleation of the system, consequentially leading to an abundance of new crystal nuclei and a diminished overall grain size of the crystal. Conversely, incorporation of a larger quantity of seeds will stimulate the nucleation of the system, resulting in numerous new crystal nuclei and a narrower overall crystal size [29]. When the quantity of crystal seeds added is appropriate, the supersaturation consumed by the crystal seeds in the system is only used for growth, and the crystal particle size becomes larger and larger. From Figure 9,

it can be seen that the explosive nucleation of $Sr(OH)_2 \cdot 8H_2O$ crystals after adding a large number of crystal seeds also confirms this statement.

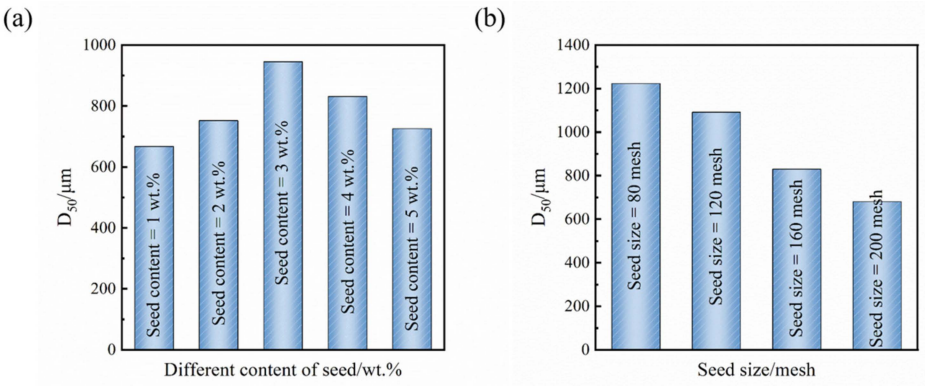


Figure 8. $Sr(OH)_2 \cdot 8H_2O$ crystal D_{50}: (**a**) for a seed crystal with a size of 120 mesh, different seed addition amounts; (**b**) at a seed addition rate of 3 wt%, different seed sizes.

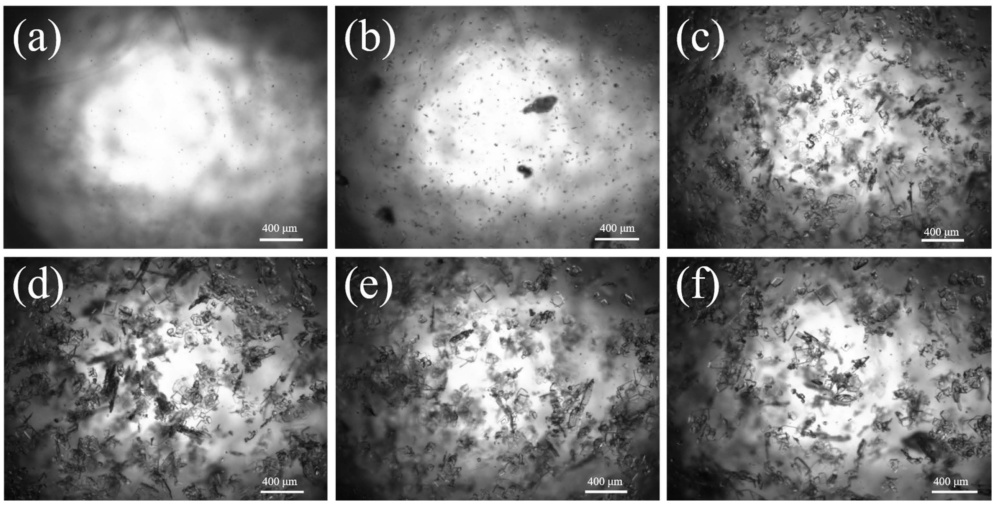


Figure 9. Images of explosive nucleation after seed addition; (**a**) 0 min, (**b**) 20 min, (**c**) 40 min, (**d**) 60 min, (**e**) 80 min, (**f**) 100 min.

From Figure 8b, it can be seen that as the seed size increases, the crystal size of $Sr(OH)_2 \cdot 8H_2O$ increases. The D_{50} of the product achieved via 80 mesh sifting of crystal seeds measures 1223 μm. The crystal seeds themselves possess a considerable size and continue to expand under the influence of supersaturation, further augmenting the size of the crystal seeds [36]. This is because under the same amount of seed addition, the smaller the seed particles, the more seeds there are, and the higher the probability of crystal nucleation in the solution under the action of surface energy, resulting in a relatively small crystal particle size; conversely, the larger the seed grain size, the larger the particle size of the attained product.

3.6. PAT and Regulatory Mechanism of Seed Crystal Regulation

Under the conditions described in Section 3.4, we added 80 mesh 3 wt% crystal seeds to the metastable region to explore the seed control mechanism of $Sr(OH)_2 \cdot 8H_2O$. Figure 10a depicts the turbidity variation in $Sr(OH)_2 \cdot 8H_2O$ during the crystallization process under optimized parameters after adding crystal seeds. Upon the inclusion of crystal seeds, the turbidity of the solution escalated; however, the system did not precipitate instantly. Following an interval of equilibrium, the turbidity persisted progressively escalating without explosive nucleation. The curve depicting turbidity in the diagram does not ascend linearly

as the crystal seeds immobilize nucleation constituents, reducing the supersaturation of the system. Moreover, the addition of crystal seeds provides growth sites for $Sr(OH)_2 \cdot 8H_2O$ crystals, thereby avoiding the occurrence of explosive nucleation. According to the size distribution curves measured with the ultrasonic particle size device at different time points in Figure 10b, it can be seen that after the addition of crystal seeds, the particle size measured with this system is the crystal seed size. The supersaturation of the initial system is consumed by the crystal seeds for growth, and the nucleation effect is mitigated; thus, no crystal nuclei are produced. As the system temperature further decreases, the supersaturation in the solution cannot be consumed entirely via crystal growth, leading to secondary nucleation in the system. It can be seen that the particle size distribution at 25 min is broader than that at 15 min, which is attributed to the formation of new crystal nuclei.

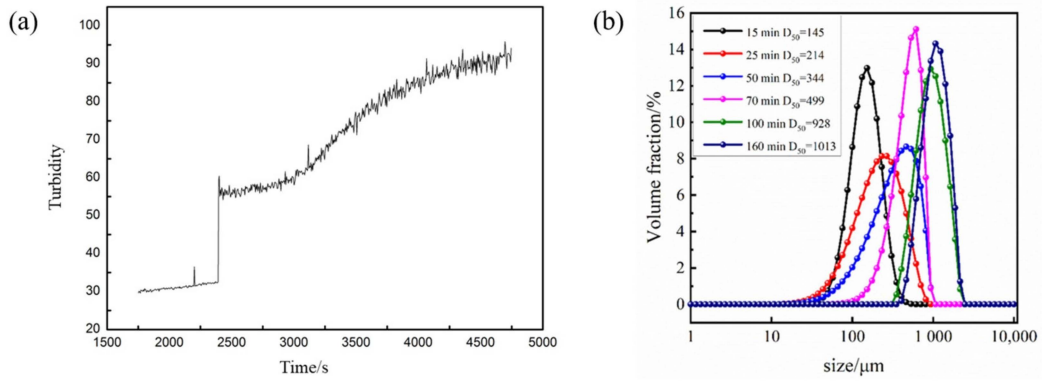


Figure 10. (**a**) Turbidity change curve after adding crystal seeds. (**b**) Particle size distribution of $Sr(OH)_2 \cdot 8H_2O$ at different times.

The generation of crystal nuclei has already consumed a portion of supersaturation, and as the crystal size gradually increases, the supersaturation in the system is further consumed. When the generation rate of supersaturation in the system is less than the consumption rate of crystal growth, crystal growth gradually decelerates, resulting in a more compact distribution of crystal particle size and an enhancement in crystal particle size. Ultimately, the D_{50} of $Sr(OH)_2 \cdot 8H_2O$ can reach 1013 μm. Figure 11 shows the evolution of particles over time captured using 2D imaging. No apparent explosive nucleation phenomenon was found in the image; it displays a classic seed growth process. The nucleation components continue to grow on the surface of the crystal seed, resulting in a much larger particle size of the obtained $Sr(OH)_2 \cdot 8H_2O$ product compared with the product obtained without the crystal seed process.

The seed control process of $Sr(OH)_2 \cdot 8H_2O$ particles is a typical secondary nucleation process. It is mainly divided into three stages: "seed addition and growth", "seed-induced secondary nucleation", and "new nuclei and seed continued growth". During the initial phase, following the introduction of crystal seeds into the system, the supersaturation present in the solvent is utilized for the development of these seeds, leading to an inevitable progression in the size of the seeds. The most crucial aspect during this phase is not to cause explosive nucleation. The subsequent phase principally provokes secondary nucleation within the system under the existence of seed crystals by accumulating a suitable number of crystal nuclei to furnish sufficient growth sites. The concluding phase predominantly encompasses the sustained growth of new crystal nuclei and seeds within the system by resorting to supersaturation. The pivotal element of this phase lies in that the supersaturation generated by cooling the solution is less than that consumed by growth, implying that all supersaturation is used for growth, and no new crystal nuclei emerge. Consequently, the growth of large-particle $Sr(OH)_2 \cdot 8H_2O$ under seed control can be summarized as a "growth-nucleation-growth" mechanism.

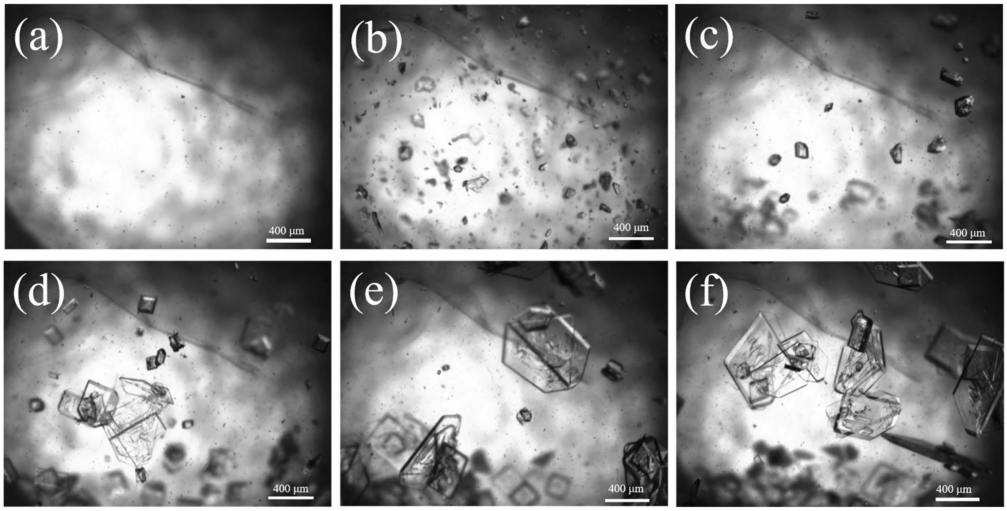


Figure 11. Two-dimensional imaging images of $Sr(OH)_2 \cdot 8H_2O$ at different times; (**a**) 0 min, (**b**) 20 min, (**c**) 40 min, (**d**) 60 min, (**e**) 80 min, (**f**) 100 min.

4. Conclusions

This study employed the utilization of PAT to fabricate a high-particle-size $Sr(OH)_2 \cdot 8H_2O$ crystal. Initially, using a hot-stage microscope, the growth process of single crystal seeds was studied by introducing them, and the average growth rate of single crystals was obtained, providing a basis for PAT research on the online growth process of $Sr(OH)_2 \cdot 8H_2O$. Subsequently, the most conducive process conditions without incorporating crystal seedlings were examined utilizing PAT: initial relative supersaturation of 3, cooling rate of 20 $^{\circ}C \cdot h^{-1}$, stirring at 150 rpm, and crystal growth for 1 h. Under these process conditions, the D_{50} of $Sr(OH)_2 \cdot 8H_2O$ crystals can be obtained, which can reach over 400 μm. Ultimately, based on the above research, $Sr(OH)_2 \cdot 8H_2O$ crystal particles with a length of over 1000 μm were prepared by optimizing the addition of crystal seeds. The $Sr(OH)_2 \cdot 8H_2O$ crystal seed regulation process was proposed as a "growth-nucleation-growth" mechanism, thus providing a theoretical research foundation and methodological reference for the high-value utilization of large $Sr(OH)_2 \cdot 8H_2O$ crystals and strontium salts.

Author Contributions: Data curation, B.S., Y.Z. and S.L.; Writing—original draft, B.S. and Y.Z.; Writing—review & editing, S.L., Y.W. and X.Z.; Supervision, Y.J., X.Z. and X.W.; Project administration, X.Z. and X.W. All authors have read and agreed to the published version of the manuscript.

Funding: This research was generously supported by the Natural Science Foundation of Qinghai Province-Youth Project (2021-ZJ-965Q), the Kunlun Talent Action Plan of Qinghai Province (E140GC4301), and the China Scholarship Council (202004910103).

Data Availability Statement: All data generated or analyzed during this study are contained in this article.

Conflicts of Interest: The authors declare no conflict of interest.

References

1. Polat, S. An in vitro evaluation of the effects of Urtica dioica and Fructus Urtica Piluliferae extracts on the crystallization of calcium oxalate. *J. Cryst. Growth* **2019**, *522*, 92–102. [CrossRef]
2. Giulietti, M.; Seckler, M.M.; Derenzo, S.; Ré, M.I.; Cekinski, E. Industrial Crystallization and Precipitation from Solutions: State of the Technique. *Braz. J. Chem. Eng.* **2001**, *18*, 423–440. [CrossRef]
3. Zhang, R.; Ma, C.Y.; Liu, J.J.; Wang, X.Z. On-line measurement of the real size and shape of crystals in stirred tank crystalliser using non-invasive stereo vision imaging. *Chem. Eng. Sci.* **2015**, *137*, 9–21. [CrossRef]
4. Ma, Y.; Qin, X.; Yan, H.; Li, J.; Li, C.; Lian, M.; Wei, X.; Shen, R.; Chen, M.; Li, K.; et al. Research Progress in the Industrial Crystallization of Citrate—A Review. *Crystals* **2023**, *13*, 1186. [CrossRef]

5. Yan, E.K.; Zhao, F.Z.; Zhang, C.Y.; Yang, X.Z.; Shi, M.; He, J.; Liu, Y.L.; Liu, Y.; Hou, H.; Yin, D.C. Seeding Protein Crystallization with Cross-Linked Protein. *Cryst. Cryst. Growth Des.* **2018**, *18*, 1090–1100. [CrossRef]
6. De Yoreo, J.J.; Gilbert, P.U.; Sommerdijk, N.A.J.M.; Penn, R.L.; Whitelam, S.; Joester, D.; Zhang, H.; Rimer, J.D.; Navrotsky, A.; Banfield, J.F.; et al. Crystallization by particle attachment in synthetic, biogenic, and geologic environments. *Science* **2015**, *349*, 6247. [CrossRef] [PubMed]
7. Dandekar, P.; Kuvadia, Z.B.; Doherty, M.F. Engineering Crystal Morphology. *Annu. Rev. Mater. Res.* **2013**, *43*, 359–386. [CrossRef]
8. Yu, Z.Q.; Chew, J.W.; Chow, P.S.; Tan, R.B.H. Recent Advances in Crystallization Control. *Chem. Eng. Res. Des.* **2007**, *85*, 893–905. [CrossRef]
9. Darmali, C.; Mansouri, S.; Yazdanpanah, N.; Woo, M.W. Mechanisms and Control of Impurities in Continuous Crystallization: A Review. *Ind. Eng. Chem. Res.* **2018**, *58*, 1463–1479. [CrossRef]
10. Alvarez, A.J.; Myerson, A.S. Continuous Plug Flow Crystallization of Pharmaceutical Compounds. *Cryst. Growth Des.* **2010**, *10*, 2219–2228. [CrossRef]
11. Mascia, S.; Heider, P.L.; Zhang, H.; Lakerveld, R.; Benyahia, B.; Barton, P.I.; Braatz, R.D.; Cooney, C.L.; Evans, J.M.B.; Jamison, T.F.; et al. End-to-End Continuous Manufacturing of Pharmaceuticals: Integrated Synthesis, Purification, and Final Dosage Formation. *Angew. Chem. Int. Ed.* **2013**, *52*, 12359–12363. [CrossRef] [PubMed]
12. Simone, E.; Zhang, W.; Nagy, Z.K. Analysis of the crystallization process of a biopharmaceutical compound in the presence of impurities using process analytical technology (PAT) tools. *J. Chem. Technol. Biotechnol.* **2016**, *91*, 1461–1470. [CrossRef]
13. Yu, L. Applications of process analytical technology to crystallization processes. *Adv. Drug Deliv. Rev.* **2004**, *56*, 349–369. [CrossRef] [PubMed]
14. Malwade, C.R.; Qu, H. Process Analytical Technology for Crystallization of Active Pharmaceutical Ingredients. *Curr. Pharm. Des.* **2018**, *24*, 2456–2472. [CrossRef] [PubMed]
15. Chanda, A.; Daly, A.M.; Foley, D.A.; LaPack, M.A.; Mukherjee, S.; Orr, J.D.; Reid, G.L.; Thompson, D.R.; Ward, H.W. Industry Perspectives on Process Analytical Technology: Tools and Applications in API Development. *Org. Process Res. Dev.* **2014**, *19*, 63–83. [CrossRef]
16. Zhang, B.; Zang, H.C.; Zhong, L.; Ma, X.B.; Wang, H.W.; Zhang, H.; Li, L. Review of the Application of PAT in the Pharmaceutical Continuous Crystallization Process. *Curr. Top. Med. Chem.* **2023**, *23*, 1699–1714.
17. Liu, Y.M.; Gao, Z.Y. Study on the Preparation of High Purity Strontium Carbonate from Sr $(OH)_2 \cdot 8H_2O$. *Guizhou Chem. Ind.* **2001**, *26*, 23–25.
18. Wu, C.X. $Sr(OH)_2$ Production Process and Market Analysis. *Inorg. Salt Ind.* **2010**, *42*, 5–7.
19. Wu, S.M.; Sheng, R.P.; Gu, T. Synthesis of Narrow Distribution Nonphenylalcohol Ether. *Chem. World* **1997**, *38*, 2.
20. Luo, M.J. Process and Engineering Design of Preparation of Strontium Hydroxide from Celestial Blue Stone. Master's Thesis, East China University of Science and Technology, Shanghai, China, 2013.
21. Dean, J.A. *Lange's Handbook of Chemistry*, 15th ed.; Chinese Edition; Science Press: Beijing, China, 2000; p. 718.
22. Wang, X.Z.; Roberts, K.J.; Ma, C. Crystal growth measurement using 2D and 3D imaging and the perspectives for shape control. *Chem. Eng. Sci.* **2008**, *63*, 1173–1184. [CrossRef]
23. Nagy, Z.K.; Fevotte, G.; Kramer, H.; Simon, L.L. Recent advances in the monitoring, modelling and control of crystallization systems. *Chem. Eng. Res. Des.* **2013**, *91*, 1903–1922. [CrossRef]
24. Tang, X.H.; Li, Y.; Liu, J.J.; Zhang, Y.; Wang, X.Z. Process Analytical Technology (PAT) Aided Identification of Operational Spaces Leading to Tailored Crystal Size Distributions in Azithromycin Crystallization via Coordinated Cooling and Solution Mediated Phase Transition. *Org. Process Res. Dev.* **2017**, *21*, 1963–1971. [CrossRef]
25. Falola, A.A.; Huang, M.X.; Zou, X.W.; Wang, X.Z. Characterization of particle size distribution in slurries using ultrasonic attenuation spectroscopy: Addressing challenges of unknown physical properties. *Powder Technol.* **2021**, *392*, 394–401. [CrossRef]
26. Zhong, X.; Huang, C.; Chen, L.; Yang, Q.; Huang, Y. Effect of ultrasound on the kinetics of anti-solvent crystallization of sucrose. *Ultrason. Sonochem.* **2022**, *82*, 105886. [CrossRef] [PubMed]
27. Hatkar, U.N.; Gogate, P.R. Process intensification of anti-solvent crystallization of salicylic acid using ultrasonic irradiations. *Chem. Eng. Process. Process Intensif.* **2012**, *57–58*, 16–24. [CrossRef]
28. Chikan, V.; McLaurin, E. Rapid Nanoparticle Synthesis by Magnetic and Microwave Heating. *Nanomaterials* **2016**, *6*, 85. [CrossRef]
29. Ji, Z.; Wang, X.; Zhang, H.; Lin, S.; Meng, H.; Sun, B.; George, S.; Xia, T.; Nel, A.E.; Zink, J.I. Designed Synthesis of CeO_2 Nanorods and Nanowires for Studying Toxicological Effects of High Aspect Ratio Nanomaterials. *ACS Nano* **2012**, *6*, 5366–5380. [CrossRef]
30. Wang, Z.; Chen, J.F.; Le, Y.; Shen, Z.G. Preparation of Ultrafine Beclomethasone Dipropionate Drug Powder byAntisolvent Precipitation. *Ind. Eng. Chem. Res.* **2007**, *46*, 4839–4845. [CrossRef]
31. Zhang, H.X.; Wang, J.X.; Zhang, Z.B.; Le, Y.; Shen, Z.G.; Chen, J.F. Micronization of atorvastatin calcium by antisolvent precipitation process. *Int. J. Pharm.* **2009**, *374*, 106–113. [CrossRef]
32. Zu, Y.; Sun, W.; Zhao, X.; Wang, W.; Li, Y.; Ge, Y.; Liu, Y.; Wang, K. Preparation and characterization of amorphous amphotericin B nanoparticles for oral administration through liquid antisolvent precipitation. *Eur. J. Pharm. Sci.* **2014**, *53*, 109–117. [CrossRef]
33. Sadeghpour, P.; Haghighi, M.; Ebrahimi, A. Ultrasound-assisted rapid hydrothermal design of efficient nanostructured MFI-Type aluminosilicate catalyst for methanol to propylene reaction. *Ultrason. Sonochem.* **2021**, *72*, 105416. [CrossRef] [PubMed]
34. Fang, L.; Gao, Z.; Wu, S.; Jia, S.; Wang, J.; Rohani, S.; Gong, J. Ultrasound-assisted solution crystallization of fotagliptin benzoate: Process intensification and crystal product optimization. *Ultrason. Sonochem.* **2021**, *76*, 105634. [CrossRef] [PubMed]

35. Ke, Y.; Chen, B.; Hu, M.; Zhou, N.; Huang, Z.; Meng, G. In-Situ Monitoring the SERS Spectra of para-Aminothiophenol Adsorbed on Plasmon-Tunable Au@Ag Core–Shell Nanostars. *Nanomaterials* **2022**, *12*, 1156. [CrossRef] [PubMed]
36. Cai, C.; Zhai, L.; Zou, C.; Li, Z.; Zhang, L.; Yang, Y.; Huang, S. $Cu_{1.94}S$-Assisted Growth of Wurtzite $CuInS_2$ Nanoleaves by In Situ Copper Sulfidation. *Nanoscale Res. Lett.* **2015**, *10*, 294. [CrossRef]

Disclaimer/Publisher's Note: The statements, opinions and data contained in all publications are solely those of the individual author(s) and contributor(s) and not of MDPI and/or the editor(s). MDPI and/or the editor(s) disclaim responsibility for any injury to people or property resulting from any ideas, methods, instructions or products referred to in the content.